Measuring orbital angular momentum of acoustic vortices based on Fraunhofer's diffraction*

Chao-Fan Gong(龚超凡), Jing-Jing Li(李晶晶), Kai Guo(郭凯),
Hong-Ping Zhou(周红平)†, and Zhong-Yi Guo(郭忠义)‡

School of Computer and Information, Hefei University of Technology, Hefei 230009, *China*

(Received 27 February 2020; revised manuscript received 6 May 2020; accepted manuscript online 12 June 2020)

Acoustic vortex (AV) beam is triggering the significant research interest in information and communication sciences due to its infinite and mutual orthogonal orbital angular momentums (OAMs). Therefore, measuring the topological charges of an AV beams become a task with great significance. In this work, we present a Fraunhofer diffraction (FD) pattern of an AV beam that can be used to quantitatively detect the OAMs of AV beams. We both theoretically and numerically investigate the FD patterns of AV beams passing through a multipoint interferometer (MPI). It is demonstrated that the topological charges of the AV beams can be determined from the interference intensity patterns. The proposed method may pave the way to the practical applications of AV beams.

Keywords: acoustic vortex, multipoint interferometer (MPI), topological charge, Fraunhofer diffraction (FD)

PACS: 43.60.+d, 43.30.Es **DOI:** 10.1088/1674-1056/ab9c11

1. Introduction

As is well known, a photon of an optical vortex with a phase distribution in the form of $\exp(\mathrm{i}l\theta)$ carries an orbital angular momentum (OAM) of $l\hbar$,[1–4] where θ is the azimuthal angle and l is an integer representing the topological charge. The OAM properties of optical vortices bring about widespread applications, such as optical micromanipulation,[5–7] quantum information,[8,9] optical communications,[10–21] and so on. In parallel to the development of vortex beams in optical[1–21] and electromagnetic[22–24] waves, the acoustic vortices have also shown their potential applications in both theory and experiment.[25–29] Like optical vortices, acoustic vortex (AV) has a typical characteristic that is the helical dislocation of wavefront, which can be described by the phase factor of $\exp(\mathrm{i}l\theta)$.[28–31] The AV beam has an indeterminate phase and a null pressure at the AV beam's center, which is useful for multiple applications including particle manipulation,[32] microorganism category,[33] acoustical tweezers,[34,35] subdiffraction imaging,[36] and acoustic communication.[37,38]

The generation of AV beam is the key factor for their applications. Hefner and Marston proposed a method to directly generate an ultrasonic vortex beam by using an acoustic source consisting of four-panel piezoelectric transducers.[39] Thereafter, a most common method to generate the AV beam is provided by independently modulating the phases and amplitudes of the discrete-point acoustic sources.[40,41] In addition, this phenomenon make us understand that the ideal key to the generation of acoustic OAM is a continuous spiral phase profile ranging from 0 to 2π with gradient phase increasing along the azimuthal direction. Due to the rapid development of metamaterials in sound wave manipulation,[42–48] the methods of generating acoustic vortices have become diversified. In addition to the use of acoustic metasurfaces,[49–51] many other schemes have been investigated, such as absorbing surfaces with a screw dislocation,[52] acoustic leaky wave antennas based on a ring resonator waveguide,[53,54] and spiral-shaped diffraction grating.[55,56] Another basis for the applications of AV beam is to measure their topological charges, which requires the knowledge of phase distributions around the singularity. However, it is not easy to directly obtain the phase distributions. So, like the case of optics, the measurement of acoustic OAM turns more significant. For optical vortex beam, the wave property has been employed to detect the topological charge based on the interference principle and diffraction theory.[57–60] The former case relies on coherent light source, in contrast, the latter one only depends on the size relation between the obstacles and wavelength. Sound is also a kind of wave, indicating that it is possible to measure the topological charges of AV beams by using their diffraction patterns.

In this paper, we demonstrate that the diffraction patterns of AV beams can be utilized to quantitatively measure their topological charges. For the proof of this concept, we both theoretically and numerically investigate the Fraunhofer diffraction (FD) of an AV beam passing through the designed mul-

*Project supported by the National Natural Science Foundation of China (Grant Nos. 61775050 and 11804073), the Natural Science Foundation of Anhui Province, China (Grant Nos. 1808085MF188 and 1808085QA21), and the Fundamental Research Funds for the Central Universities, China (Grant No. PA2019GDZC0098).

†Corresponding author. E-mail: ciangela@hfut.edu.cn

‡Corresponding author. E-mail: guozhongyi@hfut.edu.cn

tipoints interferometer (MPI). The far-field diffraction intensity patterns of AV beams with different topological charges are analyzed, from which the topological charges can be determined efficiently. In addition, we discuss the effect of the structural parameters on the measured results. The proposed concept on the FD patterns of AV beams provides a feasible method of measuring the topological charges of AV beams.

2. Theory and simulation model

Figure 1 illustrates the typical diffraction screen, the designed MPI, which is uniformly distributed multipoints with circular symmetry. The diffraction screen is centered at the position of phase singularity of the AV beam. In this work, all numerical simulations are performed by using a home-built program based on the finite element method (FEM). The whole simulation area is set to be a cylindrical waveguide filled with water. The ideal AV beam is generated directly by defining the numerical expression in our program. The ideal AV beam is incident on a 2-mm-thick diffraction screen that is placed in x–y plane at the center of a cylindrical waveguide whose radius and length are 20 mm and 150 mm, respectively. Without loss of generality, the working frequency of the incident plane acoustic wave is fixed at 300 kHz. The distance from each aperture to the center of the multipoint diffraction screen is set to be $a = 5$ mm and the radius of each aperture is assumed to be $r = 0.4$ mm. The observation plane is located at a distance of $z = 10\lambda$. The material parameters are set to be $\rho = 7800$ kg·m^{-3}, $c = 5$ km·s^{-1} for stainless steel and $\rho = 1000$ kg·m^{-3}, $c = 1.5$ km·s^{-1} for water, where ρ and c represent the mass density and sound speed, respectively. Perfectly matched layer condition is used at the waveguide boundaries to avoid producing the unphysical backward reflective waves from the outer boundaries. In the following, we will describe the FD process of AV beam for measuring their topological charges.

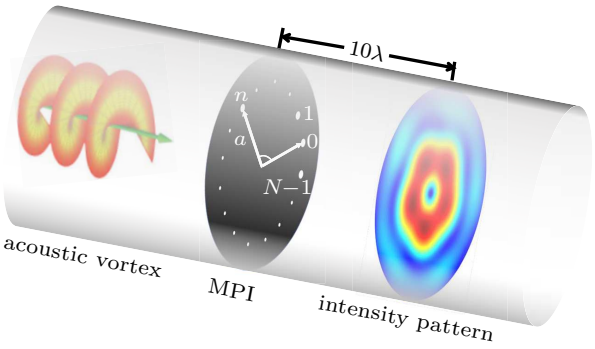

Fig. 1. Geometry and notation of generic MPI consisting of N points, uniformly distributed over a circle of radius a. The points are indicated by white dots and the angular coordinate of the n-th point is $\alpha_n = 2\pi n N^{-1}$.

We start theoretically to investigate the diffraction of the AV beams by single-circle from the MPI. In general, the MPI consists of N points which are uniformly distributed over a circle with radius of a, in which the azimuthal angle of each point can be given by $\alpha_n = 2\pi n N^{-1}$. Now, we come to consider an AV beam as an incident source. Thus, the incident phase is different at each point of the MPI. In addition, the pressure field of the AV beam can be expressed as $p = p_0 \exp(\mathrm{i}l\theta)$, where p_0 and l are the amplitude and topological charge of the AV beam, respectively. The distribution of intensity for the AV beam can be calculated from

$$I = \frac{1}{2}\frac{pp^*}{\rho c}, \tag{1}$$

where ρ and c are the mass density of the background material and sound speed in it, respectively. If the sound source is on-axis and normally incident, under the Fraunhofer's limit, the far-field intensity pattern behind the general multipoints screen can be given by the Fourier transform of the field distribution in the aperture plane as follows:[47]

$$\begin{aligned} & I_l^N(x,y,z) \propto pp^* \\ &= \left| \sum_{n=0}^{N-1} \exp(-\mathrm{i}l\alpha_n) \times \exp\left[\mathrm{i}\frac{ka}{z}(x\cos\alpha_n + y\sin\alpha_n) \right] \right|^2, \end{aligned} \tag{2}$$

where $k = 2\pi\lambda^{-1}$, and z is the distance between the multipoint screen and the observed plane.

For $N = 2$ and $l = 0$, equation (2) can be reduced to $I_0^2 \propto \cos^2(kaxz^{-1})$, resulting in a diffraction pattern similar to the central part of the results in Young's experiment with two pinholes. When the incident AV beam has an even l, the azimuthal phase dependence of the beam will introduce a phase difference of integer multiples of 2π between two points, producing a diffraction pattern the same as the case of $l = 0$. In contrast, the AV beam with an odd l will introduce a phase difference of odd multiples of π between two points, shifting the patterns of even l case by half a period. It should be mentioned that such phase differences may also be introduced by oblique incidence, making the OAM undistinguishable from a tilt of the beam. For $N = 3$, we may observe three shifted patterns repeating for $l' = l + 3$, which can also be induced by the oblique incidence. Therefore, two or three multipoints screens can only be utilized to measure the topological charge if the principal axis of the incident acoustic beam is known. For $N \geq 4$, it is not difficult to speculate that this indistinguishability will be eliminated since the phase distribution difference induced by changing of topological charge is different by nature from that induced by oblique incidences. If N approaches to infinity, equation (2) converges to the Bessel function of the first kind of order $|l|$. In other words, for $N \geq 4$, the FD pattern can be utilized to detect the topological charges of incident AV fields which will be discussed in detail in the later.

For $N \geq 4$, equation (2) can give the interesting result that the FD pattern behind a multipoint diffraction screen with

N apertures is the same as the diffraction pattern for an impinging AV beam with topological charge of l and $l' = l+N$. The diffraction pattern of AV field with topological charge of $l' = l+N$ can be described by[47]

$$\begin{aligned} I_{l+N}^{N} \propto & \left| \sum_{n=0}^{N-1} \exp\left(-\mathrm{i}\left(l+N\right)\alpha_n\right) \right. \\ & \left. \times \exp\left[\mathrm{i}\frac{ka}{z}\left(x\cos\alpha_n + y\sin\alpha_n\right)\right] \right|^2 \\ = & \left| \exp\left(\mathrm{i}\frac{ka}{z}x\right) + \exp\left(-\mathrm{i}\frac{2\pi}{N}l\right) \times \exp\left(-\mathrm{i}2\pi\right) \right. \\ & \times \exp\left(\mathrm{i}\frac{ka}{z}\left(x\cos\frac{2\pi}{N} + y\sin\frac{2\pi}{N}\right)\right) \\ & + \exp\left(-\mathrm{i}\frac{4\pi}{N}l\right) \times \exp\left(-\mathrm{i}4\pi\right) \\ & \times \exp\left(\mathrm{i}\frac{ka}{z}\left(x\cos\frac{4\pi}{N} + y\sin\frac{4\pi}{N}\right)\right) + \cdots \\ & + \exp\left(-\mathrm{i}\frac{2\pi\left(N-1\right)}{N}l\right) \times \exp\left(-\mathrm{i}2\pi\left(N-1\right)\right) \\ & \left. \times \exp\left(\mathrm{i}\frac{ka}{z}\left(x\cos\frac{2\pi\left(N-1\right)}{N} + y\sin\frac{2\pi\left(N-1\right)}{N}\right)\right) \right|^2, \end{aligned} \tag{3}$$

where $\exp\left(-\mathrm{i}2\pi\right)$, $\exp\left(-\mathrm{i}4\pi\right)$, …, $\exp\left(-\mathrm{i}2\pi\left(N-2\right)\right)$, and $\exp\left(-\mathrm{i}2\pi\left(N-1\right)\right)$ are all equal to 1. Therefore, the diffraction pattern described by Eq. (3) is identical to the diffraction pattern of the AV field with topological charge of l. In a word, the number of distinguishable l states is equal to N and the diffraction patterns are periodic in l.

For a large number of apertures N, the multipoint interferometer converges to an annular aperture and the resulting interference pattern can be described by the well-known Bessel function as

$$\lim_{N\to\infty} I_l^N\left(x,y,z\right) \propto \mathrm{J}_{|l|}\left(\frac{kar}{z}\right), \tag{4}$$

where r is the radial distance. It can be seen that the order of the Bessel function depends on the l state of the impinging AV field.

3. Results

Figure 2 shows the simulated intensities of diffraction patterns for the cases of $l = 0$, 1, 2, 3, 4 (from left to right) with $N = 4$, 5, 6, and 16 (from top to bottom) to theoretically demonstrate the performances of the proposed structures. Figure 2(a) shows that variations of l sates ($l = 0$, 1, 2, 3) result in qualitatively different patterns rather than a simple shift of the pattern. In addition, the diffraction patterns for $l = 0$ and $l = 4$ are the same as the bright spots in the center of the patterns. Thus, it can be concluded that the number of distinguishable l states therefore is equal to $N = 4$. The number of distinguishable l states increases with the number of multipoints increasing. For $N = 5$ and 6, as shown in Figs. 2(b) and 2(c), an identical conclusion can be drawn that the number of distinguishable l states is equal to $N = 5$ and 6, respectively.

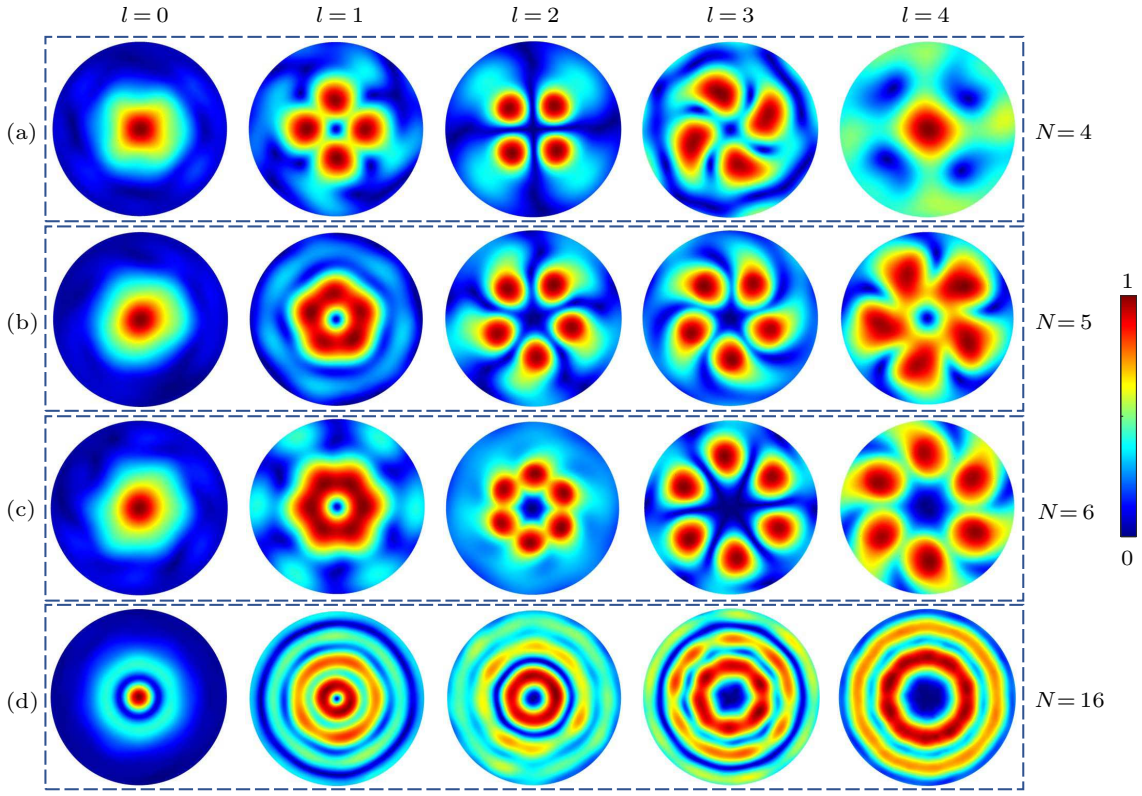

Fig. 2. Simulated far-field intensity patterns behind multipoint interferometer of N points illuminated by AV beam with topological charge l.

Figure 2(d) shows the intensities of diffraction patterns for the cases with $N = 16$, illustrating that the convergence to an annular aperture and the resulting Bessel functional diffraction pattern may happen for a relatively small topological charges. At this time, the diffraction patterns of different acoustic vortices all look similar, which is due to the insufficient precision of mesh generation when we use COMSOL. Although limited by the ability of the computer in our laboratory to carry out computing, all patterns in this case differ from each other significantly, in particular in the details surrounding the bright spots. The intensity patterns in Fig. 2 are in good agreement with theoretical analyses as mentioned above.

Figures 3(a)–3(c) show the intensities of diffraction patterns for the cases of $N = 5$ and $l = -1$, 0, and 1 respectively. Figures 3(d)–3(f) display the intensity patterns for the cases with $N = 6$ and $l = -1$, 0, and 1 respectively. It is also observed that the patterns for $l = |m|$ and $l = -|m|$ are mirrored with respect to the x axis, which can be seen from Figs. 3(a) and 3(c), which is easy to be understood since equation (2) with l and y is equivalent to that with $-l$ and $-y$. For an even N, such as $N = 6$, the diffraction patterns are symmetric with respect to the x axis, therefore reducing the number of distinguishable topological charges from N to $(N/2-1)$.

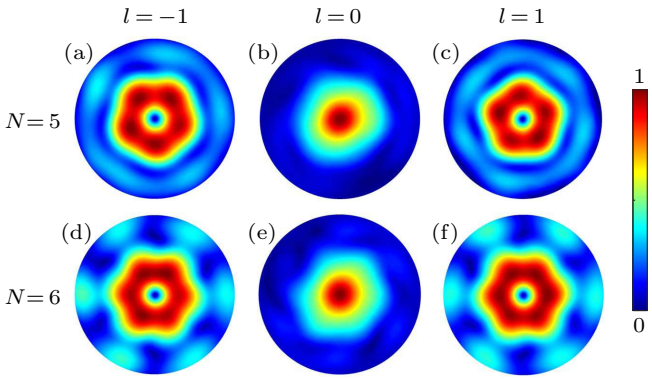

Fig. 3. Simulated far-field intensity patterns behind MPI with N points illuminated by AV beam with topological charge l, with patterns for $l = |m|$ and $l = -|m|$ being mirrored in x axis.

4. Discussion

All the above demonstrate a situation that the diffraction screens are centered at the positions of phase singularities of the acoustic beam, which are coaxially aligned. However, in general, the singularity axis of an impinging AV will not perfectly coincide with the axis of the multipoints diffraction screen. To verify the performances of our proposed method, we also investigate the influences of the displacement and tilt of the multipoints interferometer on the resulting intensity patterns. Figures 4(a) and 4(b) show the schematics of two common non-coaxial cases, *i.e.*, a displacement and a tilt of the MPI, respectively, in which d is the displacement distance and θ is the tilt angle.

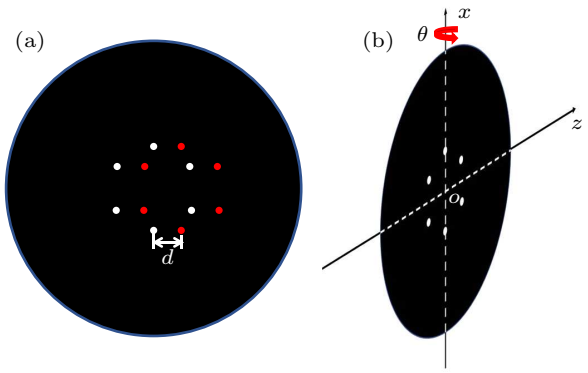

Fig. 4. (a) Displacement of MPI with respect to propagation axis of impinging beam with d for $N = 6$, and (b) MPI axis tilted with respect to the propagation axis of the impinging beam with θ for $N = 6$.

Figure 5 shows the plots of simulated diffracted far-field pattern of acoustic field intensity as a function of displacement and the tilting angle of diffraction screen with $N = 5$ pinholes. For comparison, the first column in Fig 5 is for the case where the tilt angle is set to be $\theta = 0°$, the displacements are assumed to be $d = 0$ mm, 0.3 mm, 0.6 mm, 0.9 mm (the incident wavelength in air is 1.1 mm) respectively. Without loss of generality, we simulate the case that the diffraction screen is illuminated by an AV beam with topological charge of $l = 2$. These results show that for the case with small displacements of $d = 0.3$ mm and 0.6 mm, there is no significant influence on the diffraction pattern, from which it is possible to measure the topological charges of acoustic OAM beams. In addition, large displacement of $d = 0.9$ mm blurs the observed interference patterns, making it difficult to distinguish the topological charges of incidence, as depicted in Fig. 5(d). From these simulations, we may assert that our proposed method has good robustness against the displacement of d.

Figure 5(a) shows the plots of simulated far-field diffraction patterns of the AV beams versus tilting angle $\theta = 5°$, $\theta = 10°$, $\theta = 15°$, and $\theta = 20°$ respectively. Like the above cases, the diffraction screen has $N = 5$ pinholes and the diffraction screen is illuminated by an AV beam with topological charge of $l = 2$. It is obvious that the tilt may result in significant distortion of the diffraction patterns. At a small tilting angle of $\theta = 5°$, we can still observe a similar far-field pattern to that of the coaxial case. However, when the tilt angle is larger than $\theta = 10°$, it can be seen that the diffraction pattern shifts on the observation plane with nonuniformly distributed field. When the tilting angle is set to be $\theta = 20°$, the typical feature of corresponding OAM beam almost disappears, leading to the proposed scheme to fail to measure the AV beams.

To carry out the further investigation, we simulate the noncoaxial cases in which a displacement and a tilt angle exists simultaneously. As shown in Fig. 5(b) $d = 0.3$ mm with θ from 5° to 20°, in Fig. 5(c) $d = 0.6$ mm with θ from 5° to 20°, and in Fig. 5(d) $d = 0.9$ mm with θ from 5° to 20°, when one of them increases, the diffraction pattern may be

immediately blurred. A tilt angle of $\theta = 20^\circ$ has a significant effect on the observed patterns. Similarly, for a displacement of $d = 1.1$ mm, all patterns are seriously distorted. In addition, it can be seen from a comparison between the rows from left to right that the tilting angles may have greater influence on the result than on the displacement. Fortunately, it is possible to determine the topological charge l when the displacement and tilt angle are small. Since the noncoaxial case can be corrected even avoided in experiment through carefully designing the setup, our proposed method based on the FD patterns of acoustic wave can be efficient in measuring the acoustic OAM beams.

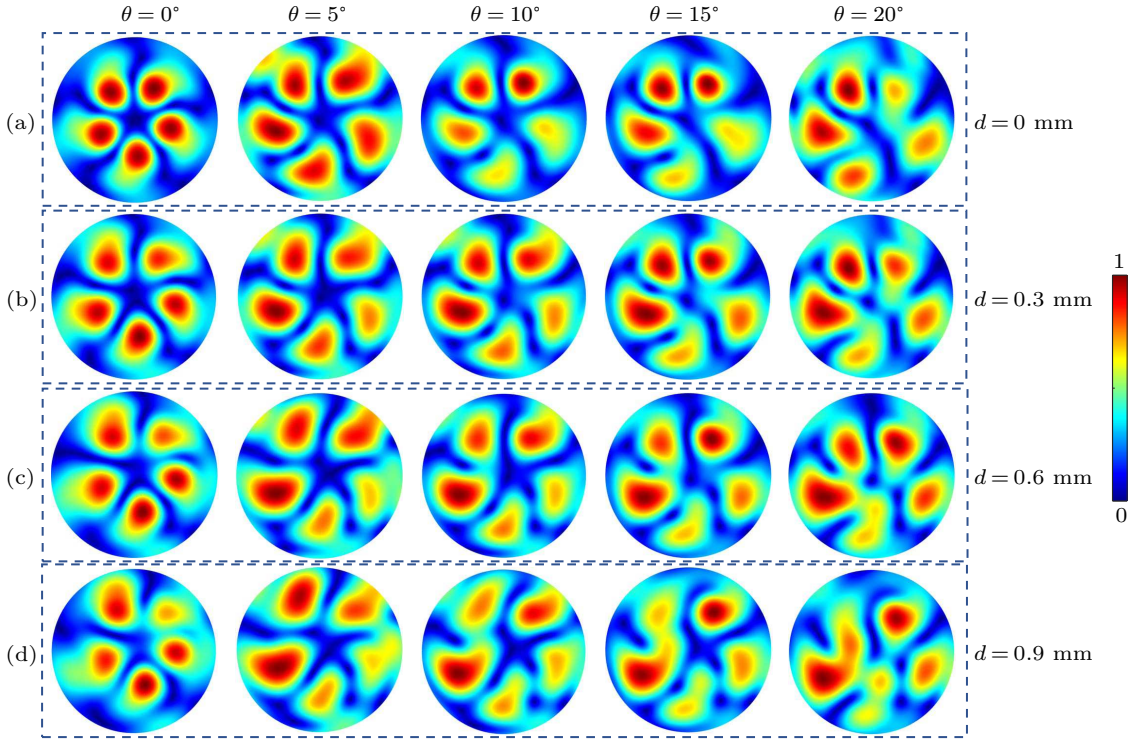

Fig. 5. Far-field intensity patterns behind a multipoint interferometer for $N = 5$ illuminated by AV with $l = 2$ displacement and tilt of the multipoint interferometer with respect to the propagation axis of impinging beam with (a) $d = 0$ mm with θ from 0° to 20°, (b) $d = 0.3$ mm with θ from 0° to 20°, (c) $d = 0.6$ mm with θ from 0° to 20°, and (d) $d = 0.9$ mm with θ from 0 ° to 20°. A displacement and a tilt of the multipoint interferometer with respect to the propagation axis of the impinging beam result in distorted and blurred interference patterns.

Overall, we propose a concept to detect the topological charge of an AV beam by using their FD patterns. We confirm its feasibility through a systematic investigation of the far-field diffraction intensity patterns with different diffraction screens and OAM modes. In fact, the diffraction pattern varies accordingly when the aperture shape changes. Unlike composite vortex,[61] the strength shape of single vortices is circular. By detecting the feature points on the FD pattern, we can obtain the topological charge of the incident acoustic vortex more easily, quickly and effectively than by detecting the acoustic vortex directly passing through the hydrophones array. It is also worth mentioning that the proposed method does not set the upper limit of the measurable topological charge according to the theory. However, with the increase of aperture number N, the types of vortex that can be detected also increase, and the differences between different modes become indistinguishable from each other. The ability of the channel to suppress the interference will be also reduced, and we can choose the appropriate MPI according to the actual needs. The results demonstrates further that it is a general method to measure AV beam by using their Fraunhofer's diffraction.

5. Conclusions

We proposed a novel concept for determining the topological charge l of the AV beam. Based on the FD patterns, the OAM of an AV beam can be measured according to the fact that different AV beams correspond to different far-field diffraction intensity patterns after the AV beam has passed through the diffraction screen. Both theoretical analyses and numerical simulations show that the FD patterns change with the topological charge l and the aperture on diffraction screen. In addition, we also discuss the effects of the tilt and displacement of multipoint interferometer on the measured results. Therefore, this concept provides a simple and feasible way to measure the topological charge of the AV beam.

References

[1] Allen L, Beijersbergen M W, Spreeuw R J C and Woerdman J P 1992 *Phys. Rev. A* **45** 8185

[2] Guo Z Y, Qu S L, Han Y H and Liu S T 2007 *Opt. Commun.* **280** 23

[3] Zhang J R, Guo Z Y, Ge C W, Wang W, Li R Z, Sun Y X, Shen F, Qu S L and Gao J 2015 *Opt. Express* **23** 17883
[4] Kai C H, Feng Z K, Dedo M I, Huang P, Guo K, Shen F, Gao J and Guo Z Y 2019 *Opt. Commun.* **430** 151
[5] Grier D G 2003 *Nature* **424** 810
[6] Zhu L, Guo Z Y, Xu Q, Zhang J R, Zhang A J, Wang W, Liu Y, Li Y, Wang X S and Qu S L 2015 *Opt. Commun.* **354** 34
[7] Liu C X, Guo Z Y, Li Y, Wang X S and Qu S L 2015 *J. Opt.* **17** 035402
[8] Inoue R, Kanai N, Yonehara T, Miyamoto Y, Koashi M and Kozuma M 2006 *Phys. Rev. A* **74** 053809
[9] Guo Z Y, Qu S L, Sun Z H and Liu S T 2008 *Chin. Phys. B* **17** 4199
[10] Wang J, Yang J Y, Fazal I M, Ahmed N, Yan Y, Huang H, Ren Y X, Yue Y, Dolinar S, Tur M and Willner A E 2012 *Nat. Photon.* **6** 488
[11] Wang Z K, Dedo M I, Guo K, Zhou K Y, Shen F, Sun Y X, Liu S T and Guo Z Y 2019 *IEEE Photon. J.* **11** 2916207
[12] Dedo M I, Wang Z K, Guo K, Sun Y X, Shen F, Zhou H P, Gao J, Sun R, Ding Z Z and Guo Z Y 2019 *Appl. Sci.* **9** 2269
[13] Guo Z Y, Wang Z K, Dedo M I and Guo K 2018 *IEEE Photon. J.* **10** 1
[14] Wang Z K and Guo Z Y 2019 *IEEE Access* **7** 163633
[15] Bozinovic N, Yue Y, Ren Y X, Tur M, Kristensen P, Huang H, Willner A E and Ramachandran S 2013 *Science* **340** 1545
[16] Yu T, Xia H, Fan Z H, Xie W K, Zhang P, Liu J S and Chen X 2018 *Acta Phys. Sin.* **67** 134203 (in Chinese)
[17] Fang G J, Sun S H and Pu J X 2012 *Acta Phys. Sin.* **61** 064210 (in Chinese)
[18] Ou J, Jiang Y S, Li F and Liu L 2011 *Acta Phys. Sin.* **60** 114203 (in Chinese)
[19] Li W, Dai S J, Ma Q Y, Guo G P and Ding H P 2018 *Chin. Phys. B* **27** 024301
[20] Ji Z Y and Zhou G Q 2017 *Chin. Phys. B* **26** 094202
[21] Cheng K, Liu P S and Lu B D 2008 *Chin. Phys. B* **17** 1743
[22] Shen F, Mu J N, Guo K and Guo Z Y 2019 *IEEE T. Antenn. Propag.* **67** 5763
[23] Yin Z Y, Zheng Q, Guo K and Guo Z Y 2019 *Appl. Sci.* **9** 2949
[24] Yang Y, Guo K, Shen F, Gong Y B and Guo Z Y 2019 *IEEE Access* **7** 138541
[25] Nye J F and Berry M V 1974 *Proc. Soc. A: Math. Phys.* **336** 165
[26] Jimenez N, Romerogarcía V, Pico R, Cebrecos A, Sanchezmorcillo V J, Garciaraffi L M, Sanchezperez J V and Staliunas K 2014 *Europhys. Lett.* **106** 24005
[27] Lekner J 2006 *J. Acoust. Soc. Am.* **120** 3475
[28] Guo Z Y, Liu H J, Zhou H, Zhou K Y, Wang X M, Shen F, Gong Y B, Gao J, Liu S T and Guo K 2019 *Phys. Rev. E* **100** 053315
[29] Zhou H P, Li J J, Guo K and Guo Z Y 2019 *J. Acoust. Soc. Am.* **146** 4237
[30] Zhang L K and Marston P L 2011 *Phys. Rev. E* **84** 065601
[31] Marston P L 2009 *J. Acoust. Soc. Am.* **125** 3539
[32] Hong Z Y, Yin J B, Zhai W, Yan N N, Wang W L, Zhang J and Drinkwater B W 2017 *Sci. Rep.* **7** 7093
[33] Ahmed D, Ozcelik A, Bojanala N, Nama N, Upadhyay A, Chen Y C, Hannarose W and Huang T J 2016 *Nat. Commun.* **7** 11085
[34] Baresch D, Thomas J and Marchiano R 2016 *Phys. Rev. Lett.* **116** 024301
[35] Wu J R 1991 *J. Acoust. Soc. Am.* **89** 2140
[36] Brunet T, Thomas J and Marchiano R 2010 *Phys. Rev. Lett.* **105** 034301
[37] Shi C Z, Dubois M, Wang Y and Zhang X 2017 *Proc. Natl. Acad. Sci. USA* **114** 7250
[38] Jiang X, Liang B, Cheng J C and Qiu C W 2018 *Adv. Mater.* **30** 1800257
[39] Hefner B T and Marston P L 1999 *J. Acoust. Soc. Am.* **106** 3313
[40] VolkeSepúlveda K, Santillan A O and Boullosa R R 2008 *Phys. Rev. Lett.* **100** 024302
[41] Demore C E M, Yang Z Y, Volovick A, Cochran S, Macdonald M P and Spalding G C 2012 *Phys. Rev. Lett.* **108** 194301
[42] Shen Y X, Peng Y G, Cai F Y, Huang K, Zhao D G, Qiu C W, Zheng H R and Zhu X F 2019 *Nat. Commun.* **10** 3411
[43] Shen Y X, Peng Y G, Zhao D G, Chen X C, Zhu J and Zhu X F 2019 *Phy. Rev. Lett.* **122** 094501
[44] Shen Y X, Zhu X F, Cai F Y, Ma T, Li F, Xia X X, Li Y C, Wang C Z and Zheng H R 2019 *Phys. Rev. Appl.* **11** 034009
[45] Tang H C, Chen Z S, Tang N, Li S F, Shen Y X, Peng Y G, Zhu X F and Zang J F 2018 *Adv. Funct. Mater.* **28** 1801127
[46] Zhu X F, Li K, Zhang P, Zhu J, Zhang J T, Tian C and Liu S C 2016 *Nat. Commun.* **7** 11731
[47] Peng Y G, Qin C Z, Zhao D G, Shen Y X, Xu X Y, Bao M, Jia H and Zhu X F 2016 *Nat. Commun.* **7** 13368
[48] Peng Y G, Li Y, Shen Y X, Geng Z G, Zhu J, Qiu C W and Zhu X F 2019 *Phys. Rev. Research* **1** 033149
[49] Jiang X, Li Y, Liang B, Cheng J C and Zhang L K 2016 *Phys. Rev. Lett.* **117** 034301
[50] Ye L P, Qiu C Y, Lu J Y, Tang K, Jia H, Ke M Z, Peng S S and Liu Z Y 2016 *AIP Adv.* **6** 085007
[51] Esfahlani H, Lissek H and Mosig J R 2017 *Phys. Rev. B* **95** 024312
[52] Gspan S, Meyer A, Bernet S and Ritschmarte M 2004 *J. Acoust. Soc. Am.* **115** 1142
[53] Naify C J, Rohde C A, Martin T P, Nicholas M, Guild M D and Orris G J 2016 *Appl. Phys. Lett.* **108** 223503
[54] Rohde C A, Naify C J, Guild M D, Martin T P, Rogers J S, Calvo D C and Orris G J 2017 *International Society for Optics and Photonics*, April 24–27, 2017, Prague, Czech Republic, p. 10170
[55] Jimenez N, Pico R, Sanchezmorcillo V J, Romerogarcía V, Garcíaraffi L M and taliunas K 2016 *Phys. Rev. E* **94** 053004
[56] Jiang X, Zhao J J, Liu S L, Liang B, Zou X Y, Yang J, Qiu C W and Cheng C J 2016 *Appl. Phys. Lett.* **108** 203501
[57] Wang Z X, Zhang N and Yuan X C 2011 *Opt. Express* **19** 482
[58] Leach J, Courtial J, Skeldon K D, S. M. Brnett S M, Frankearnold S and Padgett M J 2004 *Phys. Rev. Lett.* **92** 013601
[59] Sztul H and Alfano R R 2006 *Opt. Lett.* **31** 999
[60] Berkhout G C G and Beijersbergen M W 2008 *Phys. Rev. Lett.* **101** 100801
[61] Shi C Z, Dubois M, Wang Y and Zhang X 2017 *Proc. Natl. Acad. Sci. USA* **114** 7250